# Special Issue Communications

## Refined Empirical Line Approach for Retrieving Surface Reflectance From EO-1 ALI Images

M. Susan Moran, Ross Bryant, Chandra D. Holifield, and Stephen McElroy

***Abstract*—The refined empirical line (REL) approach was used to convert the Earth Observing 1 (EO-1) Advanced Land Imager (ALI) sensor digital number (*dn*) to surface spectral reflectance ($\rho_\lambda$). The *dn*-to-$\rho_\lambda$ relation was derived from a bright target of known reflectance in the image, and the modeled estimates of the image *dn* at $\rho_\lambda = 0$. The mean absolute percent difference ($\Delta_{\%}$) between $\rho_\lambda$ retrieved from ALI using the REL approach and ground-measured $\rho_\lambda$ for 15 targets on six dates were 42%, 6%, and 13% in the ALI visible, near-infrared (NIR), and shortwave infrared (SWIR) spectral bands, respectively. The $\Delta_{\%}$ for $\rho_\lambda$ retrieved from ALI without any atmospheric correction were 155%, 9%, and 10% for visible, NIR, and SWIR bands, respectively. For the clear, dry atmospheric conditions in Arizona, REL correction was most crucial for the dark targets in the visible bands. Given the published values of an ALI *dn* for $\rho_\lambda = 0$, the REL offers a simple approach for retrieving reflectance from multiple ALI images for temporal surface analysis.**

***Index Terms*—Atmospheric measurements, image processing, remote sensing, satellite applications.**

### I. Introduction

The Earth Observing 1 (EO-1) Advanced Land Imager (ALI) was designed and deployed to test new technology that could be used for sensors aboard the upcoming Landsat-8 platform. Compared to the Landsat-7 Enhanced Thematic Mapper Plus (ETM+), ALI provides a greater SNR, a pushbroom sensor, greater quantization, and additional wavelength bands [3]. ALI images have been acquired over urban and wildland targets throughout the world to facilitate analysis of the new technology and the new spectral bands for a wide variety of applications. This continuing analysis is often dependent on the conversion of an ALI digital number (*dn*) to surface spectral reflectance ($\rho_\lambda$) to minimize influences of atmospheric and insolation variations on sensor signal.

Several approaches have been used for *dn*-to-$\rho_\lambda$ conversion [often termed reflectance factor retrieval (RFR)]. These include the complex procedure of measuring atmospheric conditions during the satellite overpass with specialized on-site sensors and then using an atmospheric radiative transfer model (RTM) to convert the radiance measurements to surface reflectance factors (e.g., [6]). In an attempt to eliminate the need for both atmospheric measurements and the RTM, the empirical line (EL) approach has been proposed, where an empirical relationship between at-satellite radiance (or *dn*) and $\rho_\lambda$ based on within-image targets of known $\rho_\lambda$ could be used for

TABLE I
SPECTRAL DEFINITIONS FOR THE NINE EO-1 ALI MULTISPECTRAL BANDS

| Spectral Band Name | Spectral Band Range (μm) |
|---|---|
| 1p | 0.43 - 0.45 |
| 1 | 0.45 - 0.52 |
| 2 | 0.53 - 0.61 |
| 3 | 0.63 - 0.69 |
| 4 | 0.78 - 0.81 |
| 4p | 0.85 - 0.89 |
| 5p | 1.20 - 1.30 |
| 5 | 1.55 - 1.75 |
| 7 | 2.08 - 2.35 |

reported error in RFR using EL is less than 10% and depends almost exclusively on the accuracy of the characterization of the calibration targets [2], [5].

A refined EL (REL) approach was proposed to reduce the need for within-image targets and include some advantages of the RTM-based approach [4]. The REL approach derives the relation between *dn* and $\rho_\lambda$ based on one high-reflectance target within the scene, and an estimate of the image *dn* that would be associated with a surface of $\rho_\lambda = 0$. The estimate of *dn* for $\rho_\lambda = 0$ is obtained through the use of an RTM with reasonable water and aerosol models, or measurements of atmospheric conditions on a *typical* cloudless day.

In this study, estimates of an ALI *dn* for a surface of $\rho_\lambda = 0$ were computed for all 9 ALI spectral bands in the visible, near-infrared (NIR), and shortwave infrared (SWIR) spectral bands (Table I). These values, and *dn* from a bright target of known $\rho_\lambda$, were used to compute the empirical, linear *dn*-to-$\rho_\lambda$ conversions for six ALI images acquired in Arizona. The retrieved $\rho_\lambda$ from the ALI images were compared to ground-measured $\rho_\lambda$ for 15 independent targets within these images. The results of this study offer a simple method for RFR from ALI images, with an estimate of retrieval accuracy for a variety of atmospheric conditions.

### II. Materials and Methods

During 2001, six EO-1 ALI images were acquired at cropland and rangeland study sites in Arizona: the Maricopa Agricultural Center

TABLE II
ALI *DN* FOR TARGETS OF ZERO SURFACE REFLECTANCE ($\rho_\lambda$) AS COMPUTED FROM THE RADIATIVE TRANSFER MODEL (RTM) FOR SIX DATES AT MAC AND WGEW

| ALI Spectral Band | Average *dn* | Standard Deviation |
|---|---|---|
| 1p | 1399.2 | 71.6 |
| 1 | 864.7 | 44.3 |
| 2 | 371.5 | 21.1 |
| 3 | 183.3 | 13.6 |
| 4 | 70.0 | 8.1 |
| 4p | 40.9 | 5.9 |
| 5p | 3.9 | 1.6 |
| 5 | 2.2 | 1.3 |
| 7 | 0.3 | 0.2 |

0. This was converted to ALI *dn* based on the most recent ALI calibration coefficients (December 2001). The averages of *dn* for all six images in each ALI spectral band were assumed to be the best estimate of *dn* for $\rho_\lambda = 0$ (Table II).

During each overpass, an Analytical Spectral Device (ASD) full-spectrum (FS) hyperspectral spectrometer was deployed on a powered parachute. The powered parachute was flown at approximately 100 m above ground level (AGL) to avoid atmospheric attenuation of the radiance reflected from the surface. Coincident measurements of a calibrated $0.5 \times 0.5$ m Spectralon reference panel were made before and after the flight to compute $\rho_\lambda$ from the aircraft-based measurements of radiance (a detailed description of measurement protocol was given by [4]). ALI spectral bands were simulated with the ASD FS data by integrating the 0.001-$\mu$m ASD data using the normalized spectral response curves for each ALI band. Numerous measurements of $\rho_\lambda$ for selected uniform targets at MAC and WGEW were averaged to one value and the image *dn* associated with these locations were extracted from the ALI images and averaged to a single coincident value (average target size was 20 pixels). Thus, a dataset of ground-measured $\rho_\lambda$ and ALI *dn* was compiled for 21 different targets in six images (Table III).

On each date, the target with the highest ground-measured $\rho_\lambda$ in each band was chosen as "the bright target" for that image, and it was used with the *dn* in Table II to compute the REL *dn*-to-$\rho_\lambda$ relation

$$\Delta_{\lambda\mathrm{REL}} = a + b(dn) \tag{1}$$

where $\rho_{\lambda\mathrm{REL}}$ is $\rho_\lambda$ retrieved from ALI using the REL approach, and $a$ and $b$ are the offset (i.e., *dn* at $\rho_\lambda = 0$) and slope of the linear relation, respectively. All other targets were used for REL validation.

TABLE III
DATES AND LOCATIONS OF ALI IMAGE ACQUISITIONS AND DESCRIPTIONS OF GROUND TARGETS USED IN THIS STUDY

| Target # | Date | Location | Target Description |
|---|---|---|---|
| 1 | 4/22/2001 | MAC | wheat |
| 2 | | | weeds |
| 3 | | | road |
| 4 | | | hesperaloe |
| 5 | 5/24/2001 | MAC | alfalfa |
| 6 | | | alfalfa |
| 7 | | | wheat |
| 8 | | | wheat, senescent |
| 9 | 5/26/2001 | WGEW | semi-arid grassland |
| 10 | | | semi-arid grassland |
| 11 | | | semi-arid grassland |
| 12 | | | semi-arid grassland |
| 13 | | | semi-arid grassland |
| 14 | 7/27/2001 | MAC | wheat senescent |
| 15 | | | soil |
| 16 | | | cotton |
| 17 | | | alfalfa |
| 18 | 8/29/2001 | MAC | alfalfa wet |
| 19 | | | wheat stubble |
| 20 | 9/29/2001 | MAC | alfalfa |
| 21 | | | alfalfa |

and $\rho_{\lambda\mathrm{NC}}$ represents $\rho_\lambda$ retrieved from ALI with no atmospheric correction, $d$ = earth to sun distance, $I_\lambda$ = mean solar exoatmospheric spectral irradiance, and $\theta$ = solar zenith angle.

Reflectances derived using all approaches for RFR ((1)–(3)) were validated by comparison with ground-measured $\rho_\lambda$ for the 15 validation targets. The mean absolute percent difference ($\Delta_\%$) of $\rho_{\lambda\mathrm{REL}}$ and ground-measured $\rho_\lambda$ was computed as

$$\Delta_{\%\mathrm{REL}} = \frac{\left(\sum_{i=1}^{n}\left(\frac{|\rho_{\lambda\mathrm{REL}i} - \rho_{\lambda i}|}{\rho_{\lambda i}\cdot 100}\right)\right)}{n} \tag{4}$$

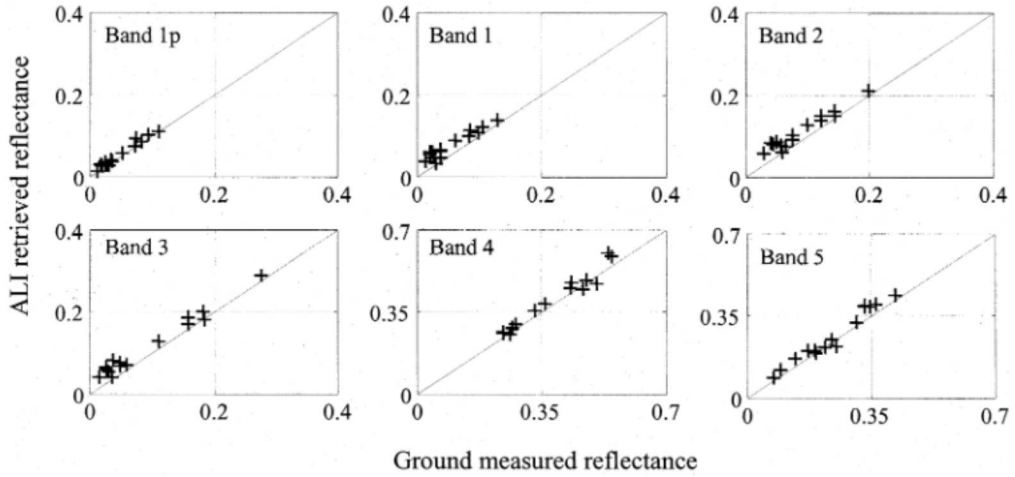


Fig. 1. Reflectance retrieved from ALI using the REL approach [(1)] compared to ground-measured reflectance for 15 targets at MAC and WGEW on six dates (from Table III). To conserve space, results from only six of nine ALI bands are presented, where band 4 represents results for the NIR spectrum, and band 5 represents results for the SWIR spectrum.

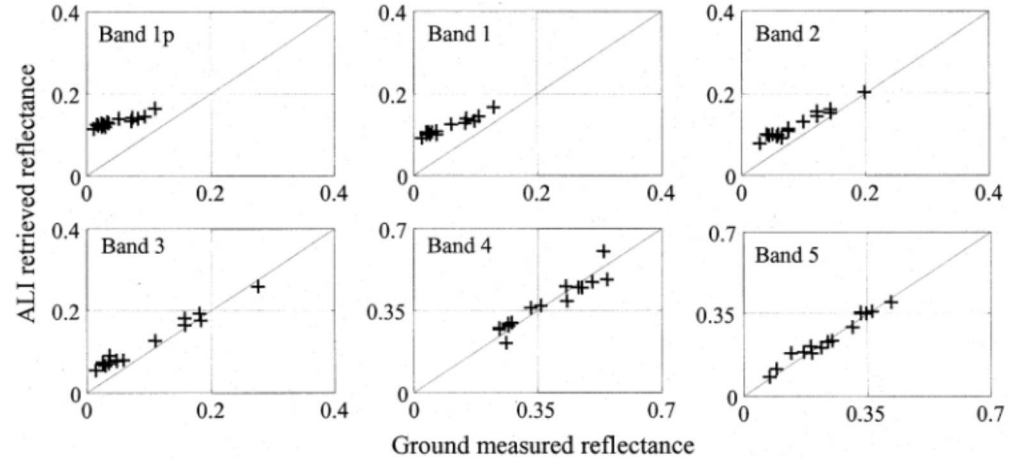


Fig. 2. Reflectance retrieved from ALI with no atmospheric correction [(3)] compared to ground-measured reflectance for 15 targets at MAC and WGEW on six dates.

The $\rho_\lambda$ retreived from ALI using the REL ($\rho_{\lambda\mathrm{REL}}$) compared well with the ground-measured $\rho_\lambda$ for the 15 targets measured during the six ALI overpasses at MAC and WGEW (Fig. 1, Table IV). Values of $\Delta_{\%\mathrm{REL}}$ ranged from 16% to 65% in the visible spectrum, 6% to 7% in NIR, and 6% to 22% in SWIR. The relatively higher $\Delta_{\%\mathrm{REL}}$ in the visible bands is largely due to the lower $\rho_\lambda$ in these bands over vegetated targets, resulting in larger $\Delta_{\%\mathrm{REL}}$ even though the absolute differences between $\rho_\lambda$ and $\rho_{\lambda\mathrm{REL}}$ were less than 0.02.

When only the bright target was used for RFR [(2)], the $\rho_{\lambda\mathrm{BT}}$ compared well with ground-measured $\rho_\lambda$ for the NIR and SWIR bands, and $\Delta_{\%\mathrm{BT}}$ was similar to $\Delta_{\%\mathrm{REL}}$ (Table IV). For the visible bands, $\Delta_{\%\mathrm{BT}}$

TABLE IV
THE MEAN ABSOLUTE PERCENT DIFFERENCE ($\Delta_{\%}$) BETWEEN GROUND-MEASURED $\rho_\lambda$ AND $\rho_\lambda$ RETRIEVED FROM ALI USING REL ($\Delta_{\%\mathrm{REL}}$), $\rho_\lambda$ RETRIEVED FROM ALI USING ONLY THE BRIGHT TARGET ($\Delta_{\%\mathrm{BT}}$), AND $\rho_\lambda$ RETRIEVED FROM ALI WITH NO ATMOSPHERIC CORRECTION ($\Delta_{\%\mathrm{NC}}$)

| ALI Spectral Band | $\Delta_{\%\mathrm{REL}}$ | $\Delta_{\%\mathrm{BT}}$ | $\Delta_{\%\mathrm{NC}}$ |
|---|---|---|---|
| 1p | 16.7 | 143.8 | 290.9 |
| 1 | 65.2 | 125.2 | 198.3 |

the accuracy of empirical line corrections (both EL and REL) depends almost exclusively on the accuracy of the characterization of the calibration targets. In our case, the corrections in the SWIR bands were very slight, and a minor inaccuracy in the measurement of $\rho_\lambda$ for the WGEW bright target resulted in an slight overcorrection of the image.

## IV. Concluding Remarks

The image-based REL approach is particularly suitable for RFR from images for which no atmospheric information is available, such as ALI images acquired around the world with minimal ground support. The values of *dn* for $\rho_{s\lambda} = 0$ derived for ALI for clear sky conditions in Arizona (Table II) could be used as a baseline for other images. That is, since these values are for a relatively clear and exceptionally dry atmosphere (columnar water vapor from 1–3 cm), REL image conversion would rarely overestimate the effects of atmospheric conditions at other sites. Obtaining $\rho_\lambda$ of a bright target for REL image correction may be more problematic, but not insurmountable. If a bright, pseudoinvariant target could be identified in the image, the bright target $\rho_\lambda$ could be measured using a handheld radiometer at the same $\theta$ for which the image of interest was acquired (methods given by [4]). Thus, the information in Table II and a good measurement of $\rho_\lambda$ of a bright target might make possible temporal and spatial analyses of archived ALI images.

## Acknowledgment

K. Thome and S. Biggar (University of Arizona Optical Science Center) provided great advice throughout the analysis.

## References

[1] R. Bryant, M. S. Moran, S. McElroy, C. D. Holifield, K. J. Thome, T. Miura, and S. F. Biggar, "Data continuity of Earth Observing 1 (EO-1) Advanced Land Imager (ALI) and Landsat TM and ETM+," *Trans. Geosci. Remote Sensing*, vol. 41, pp. 1204–1214, June 2003.

[2] V. Caselles and M. J. López García, "An alternative simple approach to estimate atmospheric correction in multitemporal studies," *Int. J. Remote Sens.*, vol. 10, pp. 1127–1134, 1989.

[3] D. E. Lencioni, C. J. Digenis, W. E. Bicknell, D. R. Hearn, and J. A. Mendenhall, "Design and performance of the EO-1 advanced land imager," in *Proc. SPIE Conf. on Sensors, Systems and Next Generation Satellites III*, Florence, Italy, Sept. 20, 1999.

[4] M. S. Moran, R. Bryant, K. Thome, W. Ni, Y. Nouvellon, M. P. Gonzalez-Dugo, J. Qi, and T. R. Clarke, "A refined empirical line approach for reflectance factor retrieval from landsat-5 TM and landsat-7 ETM+," *Remote Sens. Environ.*, vol. 78, pp. 71–82, 2001.

[5] J. R. Schott, C. Salvaggio, and W. J. Volchok, "Radiometric scene normalization using pseudoinvariant features," *Remote Sens. Environ.*, vol. 26, pp. 1–16, 1988.

[6] K. J. Thome, "Absolute radiometric calibration of Landsat 7 ETM+ using the reflectance-based method," *Remote Sens. Environ.*, vol. 78, pp. 27–38, 2001.